

Tracing the jet contribution to the mid-IR over the 2005 outburst of GRO J1655-40 via broadband spectral modeling

S. Migliari¹, J.A. Tomsick^{1,2}, S. Markoff³, E. Kalemci⁴, C.D. Bailyn⁵, M. Buxton⁶, S. Corbel⁷, R.P. Fender⁸, P. Kaaret⁹

ABSTRACT

We present new results from a multi-wavelength (radio/infrared/optical/X-ray) study of the black hole X-ray binary GRO J1655-40 during its 2005 outburst. We detected, for the first time, mid-infrared emission at $24\ \mu\text{m}$ from the compact jet of a black hole X-ray binary during its hard state, when the source shows emission from a radio compact jet as well as a strong non-thermal hard X-ray component. These detections strongly constrain the optically thick part of the synchrotron spectrum of the compact jet, which is consistent with being flat over four orders of magnitude in frequency. Moreover, using this unprecedented coverage, and especially thanks to the new Spitzer observations, we can test broadband disk and jet models during the hard state. Two of the hard state broadband spectra are reasonably well fitted using a jet model with parameters overall similar to those previously found for Cyg X-1 and GX 339-4. Differences are also present; most notably, the jet power in GRO J1655-40 appears to be a

¹Center for Astrophysics and Space Sciences, University of California San Diego, 9500 Gilman Dr., La Jolla, CA 92093-0424, USA.

²Space Sciences Laboratory/University of California Berkeley, 7 Gauss Way, Berkeley, CA 94720-7450, USA.

³ Astronomical Institute ‘Anton Pannekoek’, University of Amsterdam, Kruislaan 403, 1098 SJ, Amsterdam, The Netherlands.

⁴Sabancı University, Orhanli - Tuzla, Istanbul, 34956, Turkey

⁵Department of Astronomy, Yale University, P.O. Box 208101, New Haven, CT 06520, USA.

⁶Department of Astronomy, Columbia University, 550 West 120th Street, New York, NY 10027, USA.

⁷AIM - Unité Mixte de Recherche CEA - CNRS - Université Paris VII - UMR 7158, CEA-Saclay, Service d’Astrophysique, 91191 Gif-sur-Yvette Cedex, France.

⁸School of Physics and Astronomy, University of Southampton, Hampshire SO17 1BJ, United Kingdom.

⁹Department of Physics and Astronomy, University of Iowa, 751 Van Allen Hall, Iowa City, IA 52242, USA.

factor of at least $\sim 3-5$ higher (depending on the distance) than that of Cyg X-1 and GX 339-4 at comparable disk luminosities. Furthermore, a few discrepancies between the model and the data, previously not found for the other two black hole systems for which there was no mid-IR/IR and optical coverage, are evident, and will help to constrain and refine theoretical models.

Subject headings: X-rays: binaries - accretion, accretion disks - ISM: jets and outflows - stars: individual (GRO J1655-40)

1. Introduction

Galactic black hole (BH) X-ray binaries (XRB) spend most of their time in quiescence (a notable exception is Cyg X-1; e.g., Wilms et al. 2006), but occasionally show transient outbursts resulting in an increase in luminosity of many orders of magnitude at all wavelengths. These outbursts are explained as the result of disk instabilities, possibly due to a dramatic increase of mass accretion rate. The outbursts of BHs have been extensively monitored at all wavelengths: In the radio band, infrared (IR), optical, X-rays, and up to γ -rays. Each observing band provides distinct windows on the radiative processes related to the different components in the binary systems. In X-rays, we observe the regions of the systems close to the compact object: Inner disk, Comptonizing corona (e.g., Zdziarski et al. 1998; Nowak et al. 1999) and/or external Compton, and synchrotron self-Compton from the base of a jet (see e.g., Markoff, Nowak & Wilms 2005). In the radio band, we observe synchrotron radiation from a relativistic jet (e.g., Fender 2006 for a review). In the optical/IR band, three components may overlap: The outer and irradiated disk, the companion star, and the jet (e.g., Russell et al. 2006).

In X-rays, the different stages of an outburst can be described in terms of transitions between X-ray states. The definitions of the X-ray states are based on X-ray spectral and temporal behavior, but their details are still under debate (e.g., Homan & Belloni 2005; Homan et al. 2005; McClintock & Remillard 2006). In this work, we will follow the nomenclature in Remillard & McClintock (2006), in particular: 1) *Thermal* (or soft) state, when the disk flux fraction in the 2-20 keV energy spectrum is above 75%, the quasi-periodic oscillation (QPO) in the power density spectrum is absent or weak and the 2-10 keV power continuum has an integrated rms noise level $<7.5\%$, 2) *Hard* state, when the fraction of flux of the power-law component is $>80\%$, the power-law spectral index is $1.4 < \Gamma < 2.1$, and the power density spectrum rms is $>10\%$.

These X-ray spectral states are also associated with a specific radio (jet) behavior (see

Fender 2006 for a review). During the hard X-ray state (i.e., quiescence to rise of the outburst), the accretion rate is usually below 10% the Eddington limit and the X-ray spectrum is dominated by non-thermal power-law emission. The model to explain this non-thermal radiation is an area of controversy; the two alternate scenarios currently in consideration are a Comptonizing corona of hot electrons above an accretion disk, and Comptonizing electrons in the base of a jet, with a contribution also from synchrotron emission. A steady ‘compact jet’ is observed during this spectral state (see Fender 2006 for a recent review). The compact jet is characterized by an optically thick ($\alpha \gtrsim 0$, where $S_\nu \propto \nu^\alpha$ and S_ν is the radio flux density at a frequency ν) synchrotron radio spectrum, and it has been identified spectrally in many sources and spatially resolved in two BH XRBs: Cyg X-1 (Stirling et al. 2001) and GRS 1915+105 (Dhawan, Mirabel & Rodríguez 2000). The structure of the disc that can lead to such jet is still being debated, although magneto-hydrodynamical simulations seem to suggest a geometrically thick disc (Meier 2001). During the thermal X-ray state, the thermal component can be modeled with an optically thick, geometrically thin accretion disc (Shakura & Sunyaev 1973), the radio emission is quenched, likely due to a physical suppression of the compact jet (Fender et al. 1999; Corbel et al. 2004; Fender et al. 2004). The hard-to-soft state transition is likely associated with optically thin radio flares, a signature of the ejection of transient jets (e.g., Gallo et al. 2005).

1.1. GRO J1655-40

The BH XRB GRO J1655-40 was the second superluminal jet source discovered in our Galaxy (Tingay et al. 1995; Hjellming & Rupen 1995). The mass of the compact object has been dynamically estimated to be $M = 6.3 \pm 0.5 M_\odot$, and from the optical photometry also an inclination of the binary of $70^\circ.2 \pm 1^\circ.9$ has been derived (Greene, Bailyn & Orosz 2001). From Very Long Baseline Interferometry (VLBI) observations of the transient radio jets of GRO J1655-40, Hjellming & Rupen (1994) derived, using a distance of 3.2 kpc (in agreement with previous estimates: McKay & Kesteven 1994, Tingay et al. 1995), a jet axis inclination of $\sim 85^\circ$ to the line of sight, with a possible precession of the jet around the axis of $\sim 2^\circ$. Foellmi et al. (2006), based on the estimated optical absorption towards GRO J1655-40, have recently placed an upper limit on the distance to the source of ~ 1.7 kpc. With this new distance, the transient jets that were previously observed would no longer be superluminal. Also, using the lower distance of 1.7 kpc, the inclination of the jet axis as derived by the VLBI observations would be a few degrees lower. In this paper we will use the distance of 1.7 kpc for our calculations and fits. As a caveat, note that the distance is still under debate. Another work, still in preparation, argues that a distance greater than 3 kpc is required to explain the ellipsoidal variations observed in the optical and near infrared

(Bailyn et al. 2007, in prep.).

After seven years of quiescence, GRO J1655-40 entered a new outburst on February 2005, when the source showed an increase in the X-ray flux (Markwardt & Swank 2005), optical and near-IR magnitude (Torres et al. 2005; Buxton, Bailyn & Maitra 2005) and renewed radio activity (Rupen, Dhawan & Mioduszewski 2005a). The outburst lasted about eight months and has been extensively followed, when possible on a daily basis, at all wavelengths. In March, a state transition occurred as GRO J1655-40 entered a thermal state and the radio counterpart faded (Homan 2005; Rupen, Dhawan & Mioduszewski 2005b). In May, the source entered a highly variable, high X-ray luminosity state (Homan et al. 2005a) coupled with renewed radio emission (Rupen, Dhawan & Mioduszewski 2005c). GRO J1655-40 then entered a soft state, with no radio detection and returned to a hard state on September 23 (Homan et al. 2005b). The source returned to radio activity on September 21 (Brocksopp et al. 2005).

In this work, we present new results from a multi-wavelength (radio/infrared/optical/X-ray) campaign of GRO J1655-40 during its 2005 outburst. We study the broadband spectral energy distribution during the different stages of the outburst, with particular emphasis on the important new simultaneous observations in mid-infrared by Spitzer, which also allows for new constraints on the jet scenario. We provide an overview of the radio, mid-/near-IR, optical, soft/hard X-ray observations and data analysis in § 2; we discuss the evolution of the spectra during the outburst in § 3.1, the detection of the mid-IR emission from the compact jet in § 3.2, and the results of the fit of the broadband spectra in the context of a jet model and the discussion in § 3.3.

2. Observations

We have observed GRO J1655-40 with Multiband Imaging Photometer for Spitzer (MIPS) during its outburst that started in 2005, following the different stages from the rise of the outburst until quiescence in 2006: 1) in hard state during the rise on 2005 March 10, 2) in a thermal state after the first X-ray flux peak on 2005 April 6, 3) in a thermal state after the second and brightest X-ray flux peak on 2005 August 28, 4) during the decay of the outburst, immediately after the BH returns in the hard state on 2005 September 23 and, finally, 5) after the outburst ended, during quiescence on 2006, April 1. The arrows on top on Fig. 1, lower panel, show when these observations have been performed with respect to the 2-12 keV light curve of the All Sky Monitor (ASM) onboard the Rossi-X-ray Timing Explorer (RXTE). Since the 2005 outburst started, GRO J1655-40 has been moni-

tored daily in X-rays with pointed RXTE observations (Jeroen Homan and coworkers¹), and INTERNATIONAL Gamma-Ray Astrophysics Laboratory (INTEGRAL; Integral Galactic bulge group²), in optical/near-IR with the Small and Medium Aperture Research Telescope System (SMARTS; Michelle Buxton and Charles Bailyn³) and with a good coverage also in the radio band with the Very Large Array (VLA; Michael Rupen and coworkers⁴; see also Shaposhnikov et al. 2006). The four Spitzer/MIPS observations during the outburst (see Fig. 1, top panels) were all simultaneous with pointed RXTE, SMARTS and radio (either with the VLA or the Australia Telescope Compact Array) observations, allowing us to study the evolution of the complete broadband spectrum of the BH during the different stages. GRO J1655-40 has also been observed with the Spitzer/Infrared Array Camera (IRAC) in the hard state on September 29, simultaneously with RXTE, SMARTS and quasi-simultaneously (on 2005 October 2) with VLA observations. The Spitzer/MIPS observation in quiescence, on 2006 April 1, had no coverage at other wavelength, except for the 2-12 keV observations of the RXTE/ASM. The logs of the RXTE and Spitzer observations are shown in Table 1.

2.1. Infrared and mid-infrared: Spitzer IRAC and MIPS

We have processed the Basic Calibrated Data of the MIPS observations at 24 μm and IRAC observations at 3.6, 4.5, 5.8 and 8 μm using the software *mopex* (Makovoz & Marleau 2005). We created mosaics from the 70 and 59 frames per band obtained in the MIPS and IRAC observations, respectively. GRO J1655-40 is a few arcseconds south of an extended mid-IR emitting source, very bright at 24 μm (see Fig. 1, top panels), which enhanced the background in the region of the BH and increases the uncertainties in its flux estimates. GRO J1655-40 is observed to vary significantly over our five MIPS observations, and the mid-IR emission appears to be off when the source is in its quiescent state, on 2006 April 1. We extracted the flux density in a circular region centered at the optical coordinates of GRO J1655-40 and with a radius of 10 arcsec in the quiescent state observation, and used this flux (540 μJy) as background for the estimate of the flux density of the source in the other MIPS observations. We extracted the flux density of GRO J1655-40 in the other five MIPS observations and in the IRAC observation using aperture photometry, with a 10 arcsec radius circle. For each observation, we created the point-response functions (PRFs)

¹<http://tahti.mit.edu/opensource/1655/>

²http://isdcul3.unige.ch/Science/BULGE/SOURCES/GRO_J1655-40/GRO_J1655-40.html

³http://www.astro.yale.edu/buxton/smarts/light_curves/oir_gro.jpg

⁴<http://www.aoc.nrao.edu/%7Emrupen/XRT/GRJ1655-40/grj1655-40.shtml>

with `prf_estimate` and calculated the aperture corrections using the extracted PRF. We have corrected for interstellar extinction using $A_v = 3.72$, derived from Greene, Bailyn & Orosz (2001) and following the standard optical-to-IR interstellar extinction law (e.g., Rieke & Lebofsky 1985; Cardelli, Clayton & Mathis 1989). Note that, following Foellmi et al. (2006) instead, we would have obtained a slightly lower value of $A_v = 3.53$. We added 5% and 10% systematic errors on the estimate of the flux densities in the IRAC and 24 μm MIPS observations, respectively, to take into account the uncertainties in the photometric calibration (see Reach et al. 2005). The flux densities of the Spitzer observations are shown in Table 2.

2.2. Optical/near-infrared: SMARTS

Optical and IR monitoring of GRO J1655-40 was carried out throughout the 2005 outburst using the SMARTS consortium telescopes. Starting 2005 February 21, observations were carried out each clear night with the 1.3m telescope at CTIO, and the ANDICAM instrument. The ANDICAM (Depoy et al. 2003) is a dual-channel imager containing an optical CCD and an IR array, so simultaneous observations can be obtained from one optical (BVRI) and one IR (JHK) bandpasses. In the case of the outburst of GRO J1655-40, nightly observations were obtained in B, V, I, J and K (Buxton, Bailyn & Maitra 2005; Buxton & Bailyn 2005). The full SMARTS light curve will be presented elsewhere.

Standard flatfielding and sky subtraction procedures were applied to each night’s data, and the internal dithers in the IR were combined as described in Buxton & Bailyn (2004). Differential photometry was carried out each night with a set of reference stars in the field. Intercomparisons between reference stars of similar brightness to the source suggest a precision of < 0.02 magnitudes in BVIJ, and ≈ 0.03 magnitudes in K. Calibrations to the standard optical magnitude system were carried out using Landolt standards (Landolt 1992), several of which were observed on each photometric night, together with extinction corrections calculated from these standards over the course of the entire 2005 observing season. IR magnitudes were placed on the 2MASS system using 2MASS stars present in the field of view of GRO J1655-40. We estimate the accuracy of our standard field calibration to be better than 0.05 magnitudes in all bands. We show the apparent magnitudes, not yet de-reddened, in Table 3.

2.3. X-rays: RXTE

2.3.1. X-ray spectral analysis

We have analyzed the RXTE pointed observations performed simultaneously with our Spitzer observations. We have used the PCA `Standard2` data of the proportional counter unit 2 (PCU 2), which was on in all the observations, to produce the hardness-intensity diagram (HID) shown in Fig. 2. The hard color is defined as the count rate ratio (9.4–18.5) keV/(2.5–6.1) keV. For the energy spectral analysis, we have used PCA `Standard2` of all the PCUs available, and HEXTE `Standard Mode` cluster A and B data. For the PCA data, we have subtracted the background estimated using `pcabackest` v.3.0, produced the detector response matrix with `pcarsp` v.10.1, and analyzed the energy spectra in the range 3–25 keV. A systematic error of 0.5% was added to account for uncertainties in the calibration. For the HEXTE data, we corrected for deadtime, subtracted the background, extracted the response matrix using `FTOOLS` v.6.1.2. We have analyzed the HEXTE spectra between 20 and 200 keV. The 3–200 keV spectra are well fitted using a multicolor disk black-body, a power-law, with a cutoff for the March 10 and April 6 spectra, a smeared edge around 7–9 keV (we constrained the width of the edge to be < 15 keV) and, for the April 6 observation, a Gaussian emission line around 6.2 keV is required, possibly a red-shifted Iron line, although the energy is still marginally consistent with neutral Iron line centered at 6.4 keV. We also accounted for photoelectric absorption from interstellar material. The inner temperature of the disk is particularly low for the three hard state observations, and we fixed it to 0.5 keV because it cannot be well-constrained. Also, we fixed the equivalent hydrogen column density to $N_{\text{H}} = 8 \times 10^{21} \text{ cm}^{-2}$, a value comparable to those measured in previous observations of GRO J1655–40 (e.g., Tomsick et al. 1999). We show the best-fit parameters of each of the 3–200 keV spectra in Table 4.

2.3.2. X-ray temporal analysis

For each observation, we compute the power density spectra from the PCA data using IDL programs developed at the University of Tübingen (Pottschmidt 2002). The power density spectrum is normalized as described in Miyamoto & Kitamoto (1989) and corrected for the dead-time effects according to Zhang et al. (1995). Using 256 second time segments, we investigate the low frequency quasi-periodic oscillations (QPOs) and the timing properties of the continuum up to 100 Hz. We fit all the power density spectra with broad and narrow Lorentzians (Fig. 3) with our standard timing analysis techniques (e.g., Kalemci et al. 2005; see Belloni, Psaltis & van der Klis 2000; Nowak 2000; Pottschmidt et al. 2003). The rms

amplitudes are calculated over the whole frequency range of the power density spectrum, calculated from zero to infinity from the fitted Lorentzians, integrated over 2-15 keV. Although the aperiodic X-ray variability features are still poorly understood in detail, they are thought to be related to physical time scales in the accretion disk (see, e.g., van der Klis 2006 for a review). The multi-Lorentzian model description of the power spectra, although not necessarily physically motivated, makes it possible to identify the different components in the power density spectrum and follow their variations also in relation with other observational parameters (see Belloni, Psaltis & van der Klis 2000). These characteristics make the power density spectra a powerful (complementary) tool to classify the different observational states of the X-ray binaries. In this work, we will study the power density spectra only for classification purposes, following Remillard & McClintock (2006) and Homan & Belloni (2005) (see also van der Klis 2006). The power density spectra on April 6 and August 28 are well fitted with two broad Lorentzians, no QPOs are present and the total rms is $\lesssim 5\%$, which is typical of observations in a thermal state. More than two Lorentzians are needed to fit the more complex power density spectra of the March 10, September 24 and September 29 observations. At least three broad Lorentzians and one QPO component (plus the first harmonic of the QPO in the case of the March 10 observation) are necessary. The presence of a 0.1-10 Hz QPO and the total rms $\gtrsim 25\%$ indicate that the observations are in or very close to a hard state. We show the power density spectra of the five observations with the multi-Lorentzian fitting components in Fig. 3.

2.4. Radio: VLA

In this work, we used the VLA radio flux densities at 5 and 8.5 GHz from Shaposhnikov et al. (2006) for the 2005 March 10 observation, at 5 GHz from Brocksopp et al. (2005) for the 2005 September 22 observation, and at 5 GHz from Michael Rupen and collaborators webpage⁵ for the observations on 2005 April 6, August 28, and October 2. The radio-to-X-rays spectral energy distributions (SEDs) of the 5 observations of GRO J1655-40 are shown in Fig. 4.

⁵www.aoc.nrao.edu/~mrupen/XRT/GRJ1655-40/grj1655-40.shtml

3. Results and Discussion

3.1. The Outburst Evolution

We follow the evolution of our six observations during the outburst using the X-ray light curve (Fig. 1), the HID (Fig. 2), the power density spectra (Fig. 3) and the SEDs (Fig. 4). We inspected the PCA light curves with 16 second time resolution for the observations taken on March 10, April 6, August 28, September 24 and September 29. We do not see any long-term trends in the count rate over the duration of the observations (on a time scale of hours), or any X-ray dips or flares with amplitudes greater than $\sim 15\%$.

1) Based on the X-ray definition in Remillard & McClintock (2006), on 2005 March 10, the source is in the *hard state*. The power density spectrum shows a high rms of $\sim 34\%$ and broad features as well as a narrow QPO around 2 Hz. The X-ray energy spectra show a disk flux of $\sim 5\%$ the total 2-20 keV flux, also consistent with their definition of hard state. However, the X-ray flux already started its abrupt rise towards the first peak of the outburst. The position on the HID, if compared to those of September 24 and 29 which are also in the hard state (see below; see also Homan’s ‘open source’ page⁶ for a comparison with other GRO J1655-40 observations), suggests that the source was leaving the hard state. Indeed, if we follow the nomenclature of Homan & Belloni (2005) instead, which is based on the spectral index of the X-ray power law, and the QPO and integrated rms strength in the power density spectra, we would identify the March 10 as a *hard intermediate state* (HIMS) observation (see also Shaposhnikov et al. 2007). The radio emission is significantly detected in two bands (5 GHz and 8.6 GHz), with a spectral index of $\alpha = -0.36 \pm 0.34$; this spectral index is consistent with either a compact jet, as typically observed in hard state observations, or optically thin synchrotron emitting jet, possibly indicating that the outer part of the jet was decoupled from the system and the source had already left the hard state. Given the lack of conclusive proof, we will discuss both the hard state and HIMS classifications, where, with ‘hard state’, we also imply that a radio optically thick jet is present. An excess in the spectrum at $24 \mu\text{m}$ suggests that the jet component is dominant also in the IR band (see § 3.2 for a discussion). In case the source is in a hard state and the radio emission is from a compact jet, a power-law fit of the radio-to-IR spectrum gives an almost flat spectral index of $\alpha = 0.08 \pm 0.03$.

2) On 2005 April 6, the source is in a *thermal state*. The X-ray light curve shows that during this observation, GRO J1655-40 is in a steady high flux state, in between the two outburst peaks. The power density spectrum shows a $rms \sim 5\%$, typical of a thermal state. The

⁶<http://tahti.mit.edu/opensource/1655/>

power-law component in the X-ray spectrum is about 20% of the total 2-20 keV flux and the source is, accordingly, in the upper-left, soft region of the HID pattern. The radio emission is already quenched with a 5 GHz 3σ upper limit of 1 mJy, and the thermal emission dominates the energy spectrum in the X-ray, optical and mid-IR band: Spitzer/MIPS detected the IR tail of the bright disk at 24 μm . Note also that the hard X-ray component above ~ 30 keV disappears in this observation, going below the detection threshold of HEXTE.

3) On 2005 August 28, GRO J1655-40 is in a *thermal state*. The X-ray light curve shows that the source is still at a high flux level, but already starting its decay towards the hard state. The *rms* noise in the power density spectrum is $\sim 2\%$, typical of a thermal state, as is its position on the far left of the HID. The energy spectrum still shows a bright disk in the soft X-rays, where the disk flux is 94% of the total 2-20 keV flux. We also see the reappearance of the hard X-ray component above 30 keV. The radio emission is not detected down to a 3σ upper limit of ~ 1 mJy and the source is only marginally detected at 24 μm .

4-5) On 2005 September 24 and 29, GRO J1655-40 is observed during the decay of the outburst, when it returns to the *hard state*. The *rms* values in the power density spectra increase significantly to $\sim 25\%$ and some features, like a QPO around 0.3 Hz appears on September 24. The source reaches the bottom right part of the HID and the X-ray spectra are dominated by a non-thermal power-law component whose 2-20 keV flux is more than 90% of the total flux. The IR emission (IRAC on September 24 and MIPS on September 29) shows an excess due to the re-brightening of the jet. This jet re-brightening is clearly visible in the radio band, where its flux density at 5 GHz increases between September 24 and 29, contrary to the X-ray flux that is still decaying in time: no radio/X-ray flux positive correlation is present.

6) On 2006 April 1, the source has already returned to quiescence; no pointed RXTE, radio and optical observations are available. The Spitzer/MIPS observations does not detect the source at 24 μm .

3.2. Mid-infrared emission from the compact jet

We detect mid-IR emission at 24 μm from the hard state observations of GRO J1655-40 on September 29 and the hard (or HIMS) observation on March 10. The source is also detected on April 6, when GRO J1655-40 was in a thermal state. Thanks to the optical and near-IR simultaneous observations, we can clearly distinguish the contribution of the companion star in the binary system; its spectrum can be represented by a black body

peaking at a few 10^{14} Hz, that should show a Rayleigh-Jeans decay at lower frequencies. The comparison of the near-IR flux distribution with a power-law with spectral index 2 and normalized to the flux in the K band (1.39×10^{14} Hz), clearly shows in both the March 10 and the September 29 observation, a deviation from a Rayleigh-Jeans spectrum in the mid-IR, with an excess at $24 \mu\text{m}$. Other possible contributors to the mid-IR emission are the jet and the irradiated disk components (Cunningham 1976; Vrtilik et al. 1990; Hynes et al. 2002; see also Russell et al. 2006 for a discussion). The variability observed in the mid-IR rules out a circumbinary disk origin.

In the March 10 observation, the disk emission is significantly higher than in the other hard state observations and the contribution of the disk irradiation might be significant. Mid-IR emission is also detected during the April 6 observation, when GRO J1655-40 was in a thermal state. The disk component dominates the X-ray spectrum, and a black body the optical-IR band (see Fig. 4). The jet is not detected in the radio band with a 3σ upper limit of 1 mJy, supporting the evidence that in BHs the compact jet is suppressed during the thermal state. In this case, the mid-IR emission is most likely due to the contribution of an irradiated disk component. The $24 \mu\text{m}$ flux of the April 6 and of the March 10 observations are comparable (see Table 2). However, during the March 10 observation both the disk and the black body component are much fainter, indicating, therefore, a significant contribution in the mid-IR of another component, i.e., the jet, which is also detected in the radio band.

In the September 29 observation, the mid-IR emission is about 50% higher than on March 10 (Table 2), but the disk emission is much weaker (Table 4), strongly indicating that the compact jet, also clearly detected in the radio band, is the dominant contributor to the mid-IR. Indeed, a fit with a power-law model from the radio band to the mid-IR, gives a spectral index of $\alpha = 0.07 \pm 0.04$, consistent with a flat optically thick synchrotron emission from a compact jet. A deviation from a Rayleigh-Jeans spectrum is observed also on September 24, where an excess flux is already present at $8 \mu\text{m}$. This excess, as well as in the September 29 observation, is likely dominated by the jet.

3.3. Modeling the SEDs: New Constraints on Jet Models

Different theoretical models exist to explain the emission mechanism for BH X-ray binaries in the hard state (for a discussion, see e.g., Tomsick, Kalemci & Kaaret 2004 and references therein). One of the possibilities that we will further explore in this paper is that the compact jet, observed to produce synchrotron emission from the radio to at least the IR band, is also responsible for the hard X-ray emission, which comes from the base of the jet (e.g., Markoff, Falcke & Fender 2001; Markoff & Nowak 2004; Markoff, Nowak & Wilms

2005). Difficulties in reproducing some of the observed features seem to disfavor the direct synchrotron emission from the base of the jet as the ‘dominating’ X-ray emitting mechanism in at least a few hard state observations, as in the case of the BH 4U 1543-47 (Kalemci et al. 2005). On the other hand, Körding, Falcke & Corbel (2006), based on statistical analysis of the sample of BH systems in the ‘fundamental plane’ (Merloni, Heinz & Di Matteo 2003; Falcke, Markoff & Körding 2004; see also the discussion in Heinz 2004), pointed out that a synchrotron/jet scenario, discussed in the more updated prescription including external Compton and SSC, is still in agreement with the fundamental plane for hard state BHs. Other possible arguments against the synchrotron-only jet model as the dominant X-ray emission mechanisms in X-ray binaries, have been discussed in e.g., Maccarone (2005 and references therein). In the following, we will test the most updated version of the ‘jet model’ which includes also SSC and external inverse Compton. Other models exist to interpret the observed broadband spectra, and, to date, there are no *conclusive* arguments which favor one in particular. Yuan et al. (2005) proposed, for example, an accretion-jet model to interpret the broadband energy spectra of the BH XTE J1118+480 in hard state (the same source also successfully fitted with the earlier version of the ‘jet model’ in Markoff, Falcke & Fender 2001), where a simple synchrotron emitting compact jet is superimposed *ad hoc*, to a ‘hot accretion flow’ model fitting the X-ray spectrum (i.e., an outer thin disk coexisting with an inner Advection Dominated or Luminous-Hot Accretion Flow). In their model, the hard X-ray emission comes from the hot accretion flow through thermal Comptonization. However, this model is not yet testable statistically and self-consistently in the whole broadband spectrum. Indeed, among the different models available to test against our new broadband SEDs, the jet model described in Markoff, Nowak & Wilms (2005) is the only refined broadband model that can be tested with χ^2 statistics, from the radio band to the hard X-rays.

This jet model, in its latest prescription, has already started to be explored by fitting the broadband energy spectra of two BH XRBs in hard state. Most notably, Markoff & Nowak (2004) show that either a Comptonizing corona or synchrotron self-Compton from the base of a compact jet can fit the X-ray part of the energy spectra of Cyg X-1 and GX 339-4 in hard state with the same statistical quality. Also, the non-thermal hard tail in the X-ray spectra of GRO J1655-40 can be well fit with ‘corona’ models. The best-fit values from a simple fit using a power law to account for the hard X-ray tails are shown in Table 4. One of the advantages of the jet model is that it can interpret the whole observable broadband spectrum, from the radio band to the highest energies, in a self-consistent manner. For Cyg X-1 and GX 339-4, though, the broadband spectra analyzed in Markoff, Nowak & Wilms (2005) relied on simultaneous radio and X-ray observations, leaving the optical and IR portion of the spectrum uncovered. The mid-IR, IR and optical bands are indeed critical for testing the assumptions of the model and constraining fundamental jet model parameters.

3.3.1. *The jet model*

For a detailed discussion of the jet radiative model, we refer the reader to e.g., Markoff & Nowak (2004) and Markoff, Nowak & Wilms (2005). We recall here some fundamental assumptions and a brief description of the model, as outlined in Markoff, Nowak & Wilms (2005): (1) the total power in the jet scales proportionally with the accretion power at the inner edge of the disk, (2) the jet is expanding freely and, at the very base, is only slightly accelerated as a result of the pressure gradient, (3) the jet contains cold protons that carry most of the kinetic energy while the leptons are the dominant source of radiating energy, (4) some particles are eventually accelerated into a power-law distribution, (5) the power-law is maintained along the jet beyond the shock region. Geometrically, the base of the jet is comprised of a region with (nozzle) radius r_0 , whose lower limit is the innermost stable orbit of the disk around the black hole. The uncertainties about the physics of jet formation are absorbed by initializing parameters in this region, for the rest of the jet. The jet starts as a cylindrical flow, with constant radius r_0 . After this small nozzle region, above ~ 10 gravitational radii (r_g), the jet expands sideways at the sound speed for a proton/electron plasma (i.e., $\sim 0.4c$) and is only slightly accelerated by the resulting pressure gradient. At a distance of 10-100 r_g the particles in the jet, that started with a quasi-thermal distribution, are accelerated by into a power-law distribution.

To zeroth order (for a more detailed discussion of other cooling effects already present or not yet present in the model, see Markoff, Nowak & Wilms 2005), the resulting jet emission spectrum is the superposition of (1) an optically thick synchrotron spectrum coming from the outer regions of the jet, beyond the shock region, emitting in the radio up to likely the IR band with a flat or slightly inverted power-law spectrum, (2) an optically thin synchrotron spectrum, still coming from the post-shock region but emitting at frequencies above which the jet is transparent, which emits a power-law spectrum with a negative spectral index dependent on the electron power-law distribution, (3) an optically thin and optically thick synchrotron emission from the quasi-thermal distribution of particles coming from the pre-shock jet region, and (4) external Compton from the accretion disk plus a synchrotron self-Compton (SSC) spectrum coming from the very base of the jet, from the nozzle region. Effects of high energy cooling are added to this spectrum, so that the optically thin part synchrotron spectrum decays exponentially above a certain frequency; the maximum electron energy is calculated self-consistently for the local cooling rate. A multicolor disk blackbody is added as an independent, fitted spectral component, whose photons are included for upscattering in the jet. Note that an irradiated disk component is not yet included in this version of the code.

3.3.2. *The fits*

We focus only on the hard state observations. We fitted the energy spectra of 2005 March 10, September 24 and September 29, using the Interactive Spectral Interpretation System (ISIS; Houck & Denicola 2000). This software has two main advantages: 1) we can deal easily with broadband spectra, combining spectra with response matrices and ASCII tables listing energy channels and flux densities, without response matrices, 2) it can create model-independent unfolded spectra. We refer to the work of Nowak et al. (2005) for a detailed discussion. As in Markoff, Nowak & Wilms (2005), we started the fit manually, trying to reach a χ^2 such that $\chi^2_\nu < 10$. Then we use these parameters as a starting set of parameters for the fit with ISIS. This procedure helps to avoid that the automatic minimization in ISIS would fall in local minima. The fitting analysis, starting from the manual fitting, is a fairly long procedure that can take up to a week per spectrum.

The fitting model we used consists of three components, corrected for photoelectric absorption: 1) the disk and jet models discussed above, 2) a blackbody to model the companion star, likely a F6III-F7IV (Shahbaz et al. 1999; Israelian et al. 1999; Foellmi et al. 2006), and 3) a disk reflection component (`pexriv` in ISIS) with a single Gaussian emission line in the range 6-7 keV. The values with the best-fit parameters of September 24 and 29 spectra are shown in Table 5. We first fixed the physical parameters which can be constrained by observations. We fixed the mass of the BH to $7 M_\odot$ (Orosz & Bailyn 1997; see also Greene, Bailyn & Orosz 2000), and the distance to its most recent inferred upper limit of 1.7 kpc (Foellmi et al. 2006). In § 1.2 we noted that the upper limit of 1.7 kpc on the distance is still under debate and that there are arguments that still indicate a lower limit of 3 kpc (Bailyn et al. 2007, in prep.). A debate on the distance goes beyond the scope of this paper, and we decided primarily to use the latest published value. However, since the distance enters non-linearly in many parameters of the fitting jet model, and a simple rescaling of the best-fit values in Table 5 is not possible for all of them, for comparison, we report in Table 5 also the results of a fit to the September 29 observations, with a fixed distance of 3.2 kpc. We fixed the inclination of the jet, at first, to 75° , and then we calculated a second fit for the September 29 observation with the inclination free as this observation requires a somewhat flatter optically-thick synchrotron spectrum (see below for a more detailed discussion). An inclination of 75° is consistent with the jet axis inclination inferred from the radio lobe observations by Hjellming & Rupen (1999), revised with the new upper limit on the distance to the source of 1.7 kpc. This value is also consistent with the disk inclination of $\sim 70^\circ$ inferred by Greene, Bailyn & Orosz (2002) and allowing a disk-jet misalignment of less than 15° (e.g., Maccarone 2002). We also fixed the parameters known from previous works to fall in the same range for the other BHs (Cyg X-1, GX 339-4; this choice is made as a starting point to explore the parameter space, see also Markoff, Nowak & Wilms 2005

for discussion). The relevant fitting parameters are shown in Table 5.

3.3.3. A Comparison with other BHs

In Table 5 we show the best-fit parameters of the September 24 and 29 observations (during the decay of the outburst) using the jet model, as described above. We show the SEDs of the observations with the fitting model components in Figs 5, 6 and 7. The observation on March 10 during the rise of the outburst did not give a good fit ($\chi^2_\nu = 8.35$ (80 *d.o.f.*)), and we will discuss it in more detail in § 3.3.4. The jet model fit fairly well the data of September 24, with a $\chi^2_\nu = 1.72$ (81 *d.o.f.*), and of September 29, with a $\chi^2_\nu = 0.90$ (56 *d.o.f.*), fixing the jet inclination to 75° . Note that the high χ^2 might, at least in part, be due to the fact that the optical and IR part of the spectrum has been fitted with a simple black body spectrum, which was added as an independent component to the jet model. In the September 29 fit (Fig. 5), although the fit is good in a statistical sense, the model somewhat underestimates the radio emission. The slope of the optically-thick part of the synchrotron spectrum in the modeled jet is steeper than the slope required by the observations. In order to obtain a flatter radio-IR synchrotron spectrum, we let the jet inclination be a free parameter, and the best-fit inclination obtained is $\sim 40^\circ$ ($\chi^2_\nu = 0.94$ (55 *d.o.f.*); see Fig. 7). We would like to stress that, at this stage, the free inclination is meant to be an artificial modification to try to obtain a better by-eye fit in the radio band. A jet inclination of $\sim 40^\circ$ seems unlikely given a disk inclination of 70° (Greene, Orosz & Bailyn 2001) and the previous estimates of the jet inclination (e.g., Hjellming & Rupen 1995), even using the smaller distance in Foellmi et al. (2006). Furthermore, the uncertainties in modeling the jet emission are still too large to attempt an estimate of the jet inclination using these fits. The χ^2 values for this fit are comparable because the statistics are dominated by the X-ray and optical part of the spectrum, but there is an improvement in the fit in the radio band.

A remarkable result of these fits is that the same model that can fit well GX 339-4 and Cyg X-1 broadband spectra, seems not to reproduce equally well the optically thick part of the synchrotron emission in GRO J1655-40, which is flatter than the model predicts. Possible ways to make the radio-IR emission flatter would be 1) to have a less beamed jet (which is the case emulated in the fit by the smaller jet inclination angle), that can be due to e.g., a smaller gradient in the regions contributing to the optically thick part of the jet and 2) to have a more collimated jet, such as what may be expected in the case of magnetic collimation, which is still poorly understood and not included here.

As mentioned above, Markoff, Nowak & Wilms (2005) fitted, using the jet model, some typical hard state observations of the BH XRBs Cyg X-1 and GX 339-4, and discussed the

differences and similarities found in the best-fit parameters. In particular, they found that 1) the total initial power that goes into the jet N_j is similar for both sources; 2) Cyg X-1 seems to favor a more compact jet base, with the same radius-to-height ratio (h_0), but with $4.4 r_g < r_0 < 9.1 r_g$ for Cyg X-1 against the $9.6 r_g < r_0 < 20.2 r_g$ of GX 339-4. The smaller r_0 , with a similar N_j , reflects the higher X-ray-to-radio flux ratio of Cyg X-1 with respect to GX 339-4; 3) The temperature of the electrons in GX 339-4 is $T_e \sim 4000$ keV, a factor of two larger than in Cyg X-1; 4) the spectral index of the electron distribution p , the fraction of accelerated electrons pl_f (which was large and then fixed to 75% in this work, as suggested in their paper), and the location of the acceleration region z_{acc} (approximately 20-30 r_g) are roughly the same for the two BHs; 5) both BHs appear to have the jets close to equipartition.

Comparing the parameters of GRO J1655-40 with those of the other two BHs (Table 5), it is remarkable that most of the parameters are very similar for these three different BHs. Some differences are however present; we find that the power that GRO J1655-40 put into the jet is higher than that in the other two BHs, by a factor of > 3 (the jet power is of the same order of N_j in Table 5; see also Appendix A2 in Markoff, Nowak & Wilms 2005). Also, the nozzle radius is smaller than that of GX 339-4 and very similar to that of Cyg X-1, reflecting the higher X-ray/radio flux ratio. The electron temperature is approximately the same as that found for the other two BHs, as is the spectral index of the electron distribution. The model finds solutions for a jet close to equipartition ($k \sim 1$ in Table 5) only in the case of September 29, but only if we let the jet inclination free to adjust for the otherwise steeper optically thick radio-to-IR spectrum observed. The September 24 and 29 observations with fixed inclination to 75° , find a solution for a weakly magnetically dominated jet ($k \sim 4$ and $k \sim 5$, respectively), which is different from what found for other two BH XRBs, but close to the values found for e.g., Low-Luminosity Active Galactic Nuclei as Sgr A* and M81 (e.g., Markoff et al. 2004). Note, however, that this equipartition parameter is still not very well constrained and, also, that there is no physical reason to prefer a solution with a jet in equipartition over that of a (weakly) magnetised jet. Using a distance of 3.2 kpc, the jet power of GRO J1655-40 would be about 5 times higher than that derived in the fits of Cyg X-1 and GX 339-4 for comparable disk luminosities. The jet and the disk luminosities seem to be the only two parameters that change significantly (increase) using a distance of 3.2 kpc (see Table 5).

3.3.4. *March 10: X-rays from a corona or from the base of the jet?*

We are not able to obtain a statistically good fit for the observation on 2005 March 10. We fitted this broadband spectrum with the same model components we used for the

September observations, in order to emphasize the differences between this and the other hard state spectra. The reflection fraction parameter was left free during the fit and reached a value of $\sim 70\%$. Such a high reflection fraction is two times the one found in the September observations (Table 5, using a distance of 1.7 kpc) and is physically incompatible with a mildly relativistic beamed corona or a jet model (Belodoborov 1999; Markoff & Nowak 2004). An edge around 6-7 keV and/or a stronger iron line at a different peak energy might be needed to slightly improve the spectral fitting. However, the ‘hard state’ jet model in the present form seems not to be sufficient to describe statistically well the observed broadband data. On March 10, the source is either in a hard state or in a HIMS (according to the definitions in Remillard & McClintock 2006 or Homan & Belloni 2005, respectively). The radio emission is present and the radio spectral index is consistent with both a compact and an optically thin synchrotron jet ($\alpha = -0.36 \pm 0.34$). If the source is in a HIMS and the radio spectrum is optically thin, e.g., the outer part of the jet is already decoupled from the system and the assumption of a radio compact jet is not valid anymore, the jet model in the present form cannot be used to fit the spectrum. On the other hand, if the source is in a hard state and the radio jet is still optically thick, the almost flat radio-to-IR spectral index ($\alpha = 0.08 \pm 0.03$) is consistent with a compact jet and the jet model should in principle be able to fit this observation reasonably well, as it does for the other hard state observations of GRO J1655-40 and other BHs. The SED of March 10 seems, however, to have a very high X-ray-to-radio flux ratio – too high for the model to find a good set of parameters to reproduce it. In this case, it is tempting to claim that, therefore, at least part of the hard X-ray emission, assumed in the jet model to be produced at the base of the jet, does actually come from a physically different emitting source.

We must note that on March 10, GRO J1655-40 is already starting the X-ray rise of the outburst, the disk emission is higher than that of the other hard state spectra, and only a few days later the source is in a thermal state. Therefore, a possible explanation for the bad fit is that, e.g., the compact jet is already fading, while the accretion rate, and thus the soft X-ray emission is increasing. However, we still encounter the problem of explaining the high non-thermal hard X-ray flux in the spectrum coming from a fading jet. Given the power in the compact jet, the model cannot find a good set of parameters that reproduces the hard X-ray emission observed. Therefore, *if* the source is in a hard state with a compact radio jet, and if the other assumptions in the model are not significantly incorrect, we appear to observe an alternative source of hard X-rays, other than the jet. However, since the March 10 observation is possibly in a transitional state, a time-dependent jet model may be required in this case. Such a model is currently under development, and we plan to re-visit the March 10 SED when it is available.

4. Conclusions

We have analysed five multi-wavelength observations of GRO J1655-40 during its outburst in 2005. The unprecedented coverage from the radio band to X-rays, and especially the new inclusion of simultaneous optical/IR and mid-IR observations, allowed us to give new constraints on the jet in a BH XRB.

- We detect, for the first time, emission from a compact jet in the mid-IR, at 24 μm , with Spitzer/MIPS.
- We obtain a strong constraint on the spectral index of the compact jet, which is consistent with being flat from the radio band to the mid-IR: $\alpha = 0.07 \pm 0.04$ for the September 29 observation and, possibly (see caveats in § 3.1), $\alpha = 0.08 \pm 0.03$ for the March 10 observation.
- Using the broadband SEDs in the hard state, we tested the jet scenario. We find good fits for two out of the three hard state observations. The physical parameters of the jet are overall similar to those previously found in other two BH XRBs, Cyg X-1 and GX339-4. The most notable exception is the jet power, which seems to be a factor of at least 3-5 times higher, depending on the distance, in GRO J1655-40, for comparable disk luminosities. We also note that the radio-to-IR power-law spectrum observed seems to be somewhat flatter than the model predicts.
- The jet model does not give a good fit for the observation on March 10, which can be either in a hard state or in a hard intermediate state, depending on X-ray state definitions we adopt, and has an unconstrained radio spectral index consistent with either a compact or a detached optically thin radio jet. In the case of a hard state observation, with a compact jet emitting an almost flat spectrum from the radio band to the mid-IR, this model-data discrepancy might be explained by the presence of an alternative source of hard X-rays, other than the jet.

The results presented in this work show how the wide energy range covered by our multiwavelength campaign, with a particular key role played by the mid-IR observations, can give strong constraints on the radiative components of XRB systems. The SEDs will be further used to test improved jet models (with e.g., the inclusion of an irradiated disk, of time-dependent parameters), as well as other disk and jet models based on different scenarios (e.g., Yuan et al. 2005), as soon as they can be statistically tested over the whole broadband energy spectrum.

This work is based on observations made with the Spitzer Space Telescope, which is operated by the Jet Propulsion Laboratory, California Institute of Technology under a contract with NASA. Support for this work was provided by NASA through an award issued by JPL/Caltech (#1269434 and #1271245). The National Radio Astronomy Observatory is a facility of the National Science Foundation operated under cooperative agreement by Associated Universities, Inc. The collection and analysis of the SMARTS data reported here was supported by grant AST-0407063 from the US National Science Foundation to CDB. JAT acknowledges partial support from RXTE cycle 9 and 10 grants NNG05GB22G and NNG06GA81G.

REFERENCES

- Belloni T., Psaltis D., van der Klis M., 2002, *ApJ*, 572, 392
- Beloborodov A.M., 1999, *ApJ*, 510, L123
- Buxton M., Bailyn C.D., Maitra D., 2005, *ATel*, 408
- Buxton M., Bailyn C.D., 2005, *ATel*, 608
- Buxton M., Bailyn C.D., Maitra D., 2005, *ATel*, 418
- Buxton M., Bailyn C.D., 2004, *ApJ*, 615, 880
- Brocksopp K., et al., 2005, *ATel.*, 612
- Cardelli J.A., Clayton, G.C., Mathis, J.S., 1989, *ApJ*, 345, 245
- Corbel S., Fender R. P., Tomsick J. A., Tzioumis A. K., Tingay S., 2004, *ApJ*, 617, 1272
- Cunningham C., 1976, *ApJ*, 208, 534
- Dhawan V., Mirabel I.F., Rodríguez L.F., 2000, *ApJ*, 543, 373
- Depoy et al. 2003, *SPIE*, 4841, 827
- Fender R.P., 2006, *Compact Stellar X-Ray Sources*, eds. W.H.G. Lewin and M. van der Klis, Cambridge University Press, 381
- Fender R. P., Belloni T. M., Gallo E., 2004, *MNRAS*, 355, 1105
- Fender, R.P., 2001, *MNRAS*, 322, 31

- Fender R.P. et al., 1999, ApJ, 519, L165
- Greene, J., Bailyn, C.D., Orosz, J.A., 2001, ApJ, 554, 1297
- Hynes R. I., Haswell C. A., Chaty S., Shrader C. R., Cui W., 2002, MNRAS, 331, 169
- Heinz S., 2004, MNRAS, 355, 835
- Homan, J., 2005, ATel, 440
- Homan, J., Miller, J.M., Wijnands, R., Lewin, W.H.G., 2005a, ATel, 487
- Homan, J., Miller, J.M., Wijnands, R., Lewin, W.H.G., 2005b, ATel, 607
- Homan, J., 2005c, ATel, 440
- Houck J.C., Denicola L.A., 2000, ASPC, 216, 591
- Hjellming, R.M., Rupen, M.P., 1995, Nature, 375, 464
- Kalemci, E. et al., 2005, ApJ, 622, 508
- Landolt 1992, AJ, 104, 340
- Maccarone T.J., 2002, MNRAS, 336, 1371
- Maccarone T.J., 2005, MNRAS, 360, L68
- Makovoz, D., & Marleau, F., 2005, PASP, 117, 1113
- Markoff, S.; Nowak, M.; Falcke, H.; Maccarone, T.; Fender, R., 2004, Nuclear Physics B
Proceedings Supplements, 132, 129
- Markoff, S., Nowak, M.A., 2004, ApJ, 609, 972
- Markoff, S., Nowak, M.A., Wilms, J., 2005, ApJ, 635, 1216
- Markwardt, C.B., Swank, J.H., 2005, ATel, 414
- McClintock, J.E., & Remillard, R.A., 2006, Compact Stellar X-Ray Sources, eds. W.H.G.
Lewin and M. van der Klis, Cambridge University Press, 157, astro-ph/0306213
- Meier, D.L., 2001, ApJ, 538, L9
- Miyamoto, S., Kitamoto, S., 1989, Nature, 342, 773

- Nowak M.A., J. Wilms., Heinz S., Pooley G., Pottschmidt K., Corbel S., 2005, *ApJ*, 626, 1006
- Nowak M.A., Wilms J., Vaughan B.A., Dove J. B., Begelman M.C., 1999, *ApJ*, 522, 460
- Nowak M.A., 2000, *MNRAS*, 318, 361
- Pottschmidt K., Wilms J., Nowak M. A., Pooley G. G., Gleissner T., Heindl W. A., Smith D. M., Remillard R., Staubert R., 2003, *A&A*, 407, 1039
- Pottschmidt, K., 2002, PhD Thesis, Univ. of Tübingen
- Reach W.T., et al., 2005, *PASP*, 117, 978
- Remillard R.A., McClintock J.E., 2006, *ARA&A*, 44, 49
- Rieke G.H., Lebofsky M.J., 1985, *ApJ*, 288, 618
- Rupen, M.P., Dhawan, V., Mioduszewski, A.J., 2005a, *ATel*, 419
- Rupen, M.P., Dhawan, V., Mioduszewski, A.J., 2005b, *ATel*, 441
- Rupen, M.P., Dhawan, V., Mioduszewski, A.J., 2005c, *ATel*, 489
- Russell D. M., Fender R. P., Hynes R. I., Brocksopp C., Homan J., Jonker P. G., Buxton M. M., 2006, *MNRAS*, 371, 1334
- Shaposhnikov N., Swank J., Shrader C. R., Rupen M., Beckmann V., Markwardt C. B., Smith D. A., 2007, *ApJ*, 655, 434
- Tingay S.J., et al., 1995, *Nature*, 374, 141
- Tomsick J.A., Kaaret P., Kroeger R.A., Remillard R.A, 1999, *ApJ*, 512, 892
- Tomsick J.A., Kalemci E., Kaaret P., 2004, *ApJ*, 601, 439
- Torres M.A.P., Steeghs, D., Jonker, P., Martini, P., 2005, *ATel*, 417
- van der Klis M., 1988, in H. Ögelman and E.P.J. van den Heuvel, eds, *Proceedings of the NATO Advanced Study Institute on Timing Neutron Stars*, held in Çeşme, Izmir, Turkey, April 4–15
- Vrtilek S. D., Raymond J. C., Garcia M. R., Verbunt F., Hasinger G., Kurster M., 1990, *ApJ*, 235, 162

Wilms J, Nowak, M. A.; Pottschmidt, K.; Pooley, G. G.; Fritz, S., 2006, A&A, 447, 245

Yuan F., Cui W., Narayan R., 2005, ApJ, 620, 905

Zdziarski, A.A., Poutanen J., Mikolajewska J., Gierlinski M., Ebisawa K., Johnson W. N.,
1998, MNRAS, 301, 435

Zhang W., Jahoda K., Swank J.H., Morgan E.H., Giles A.B., 1995, ApJ, 449, 930

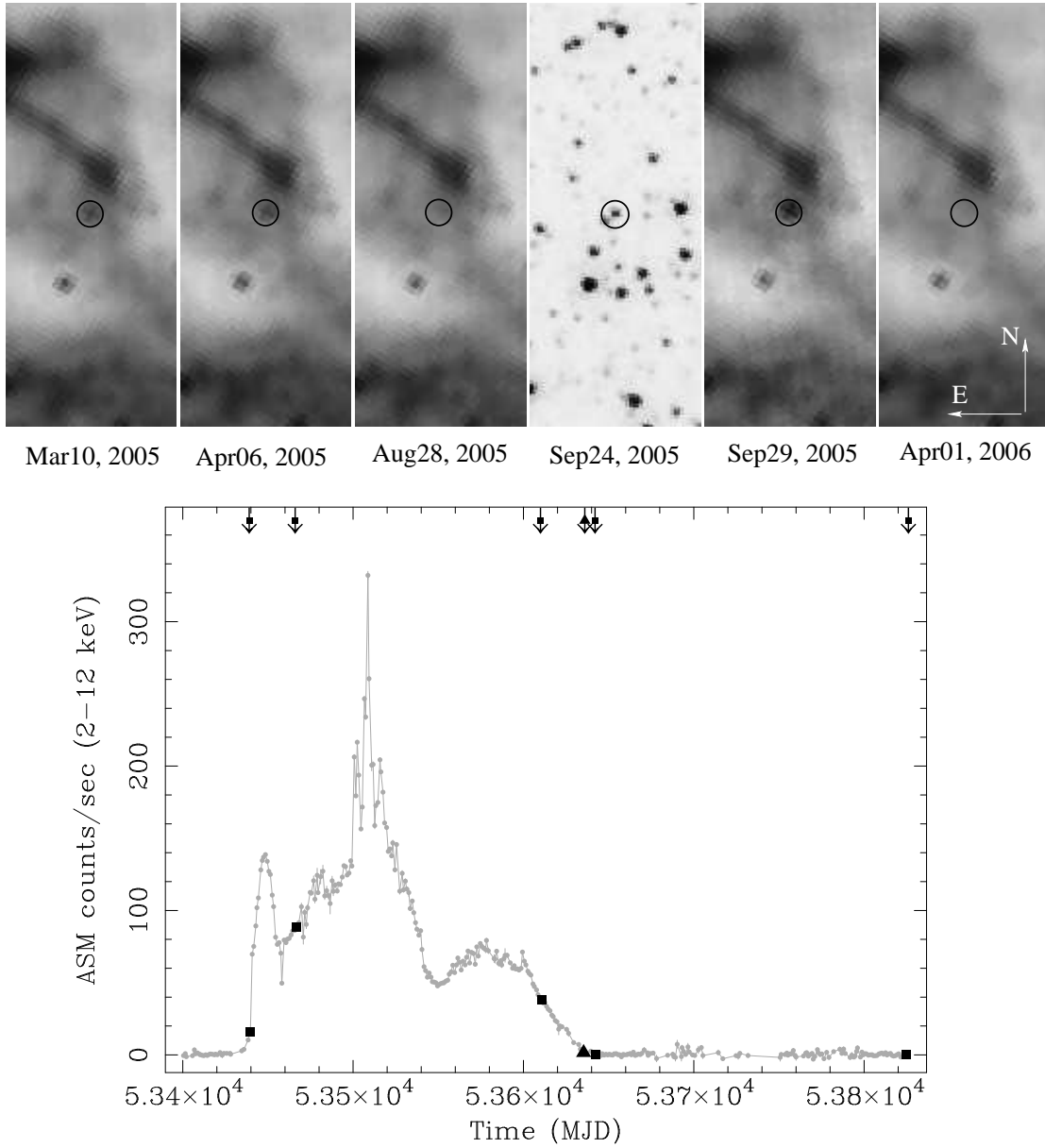


Fig. 1.— *Top panels:* Spitzer images of GRO J1655-40. All the images are taken with MIPS at $24 \mu\text{m}$, except the one on September 24 which was taken with IRAC (shown is the image at $4.5 \mu\text{m}$). The optical position of GRO J1655-40 is centered in the circle. *Lower panel:* RXTE/ASM light curve of the outburst. The squares represent the MIPS observations, the triangle shows the IRAC observation.

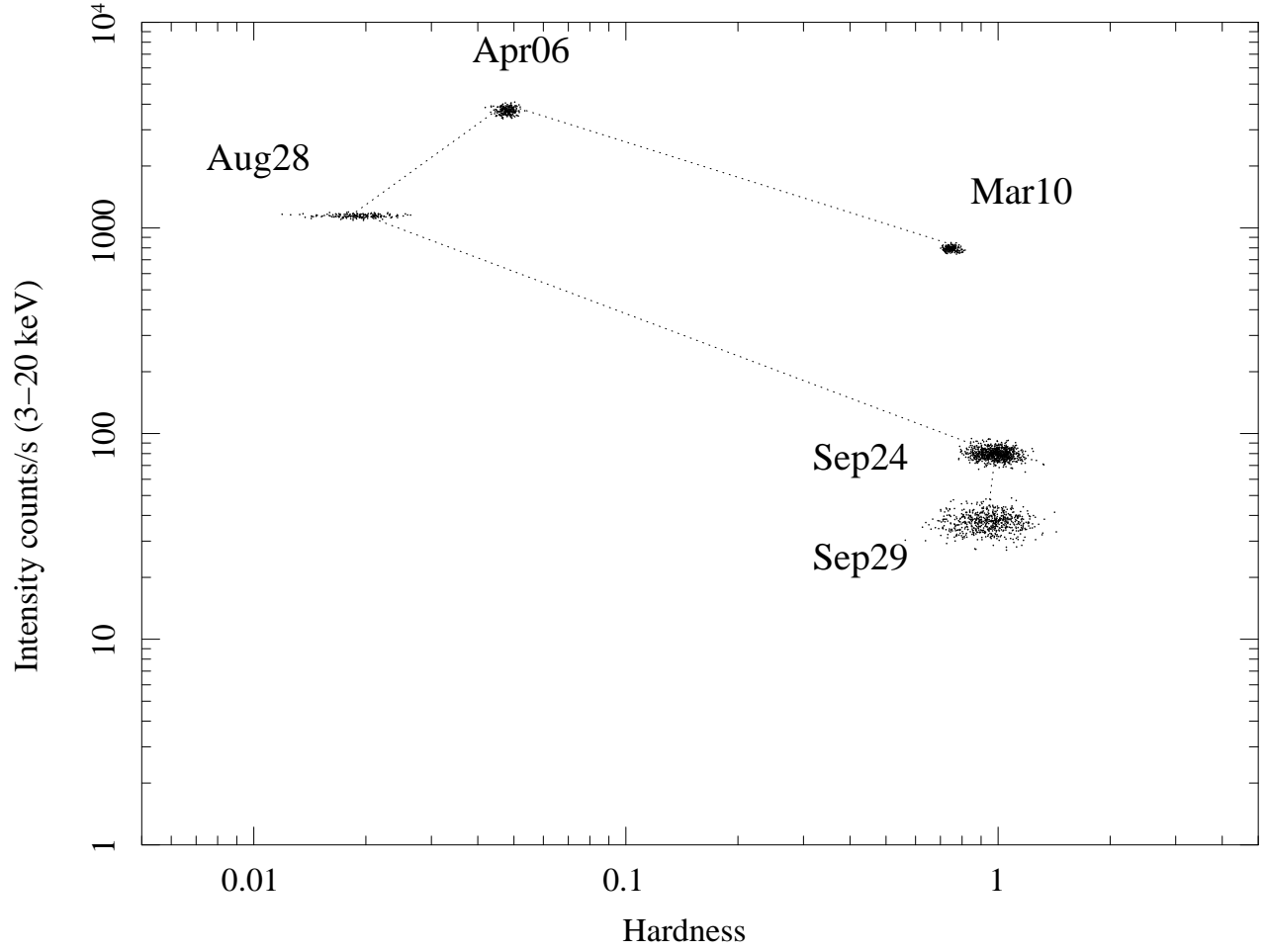


Fig. 2.— Hardness-Intensity Diagram (HID) of the five RXTE pointed observations, simultaneous with Spitzer.

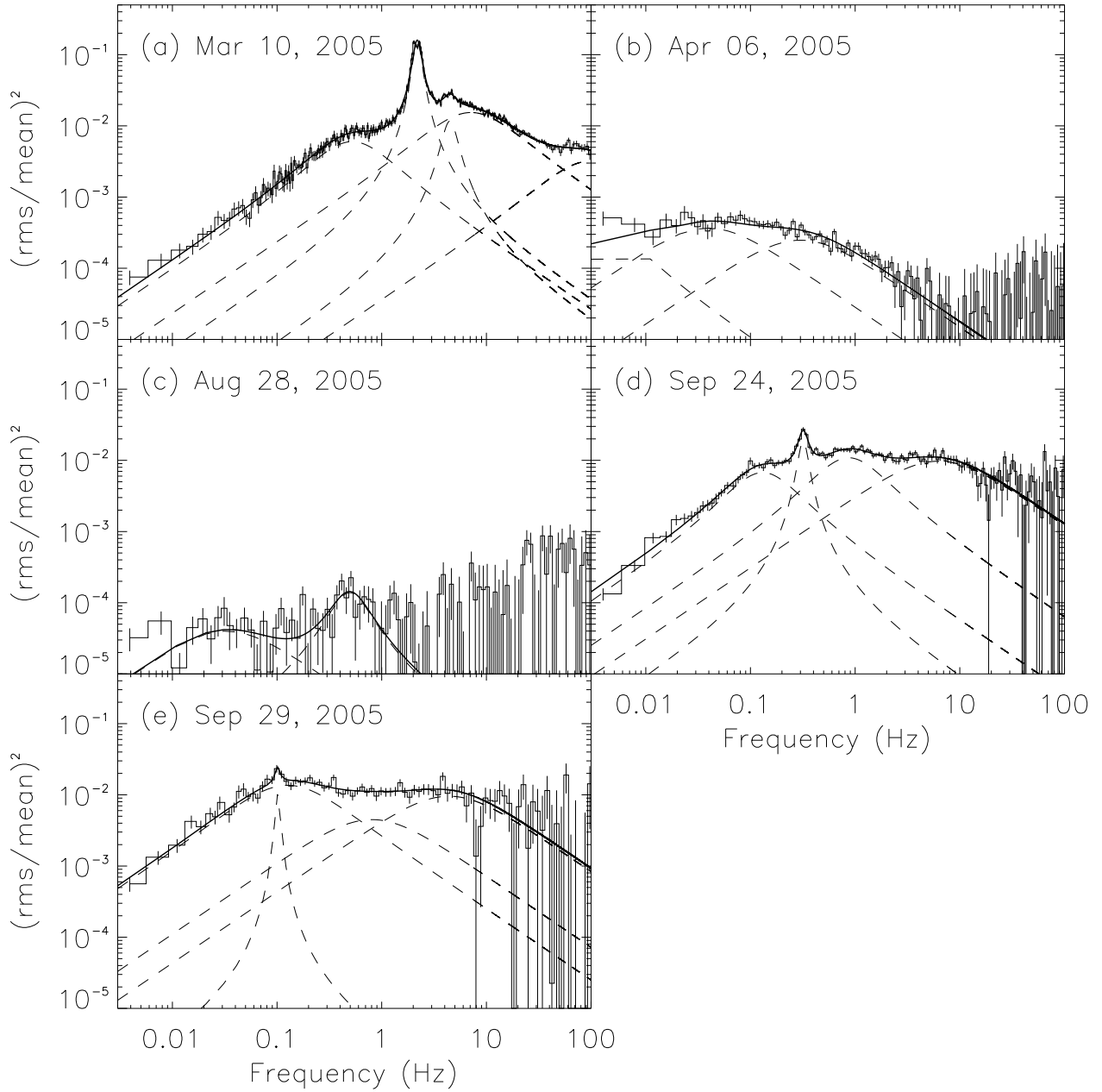


Fig. 3.— X-ray power density spectra of the five RXTE/PCA observations simultaneous with Spitzer. The dashed lines indicate individual Lorentzian components whereas the solid lines show the total fit.

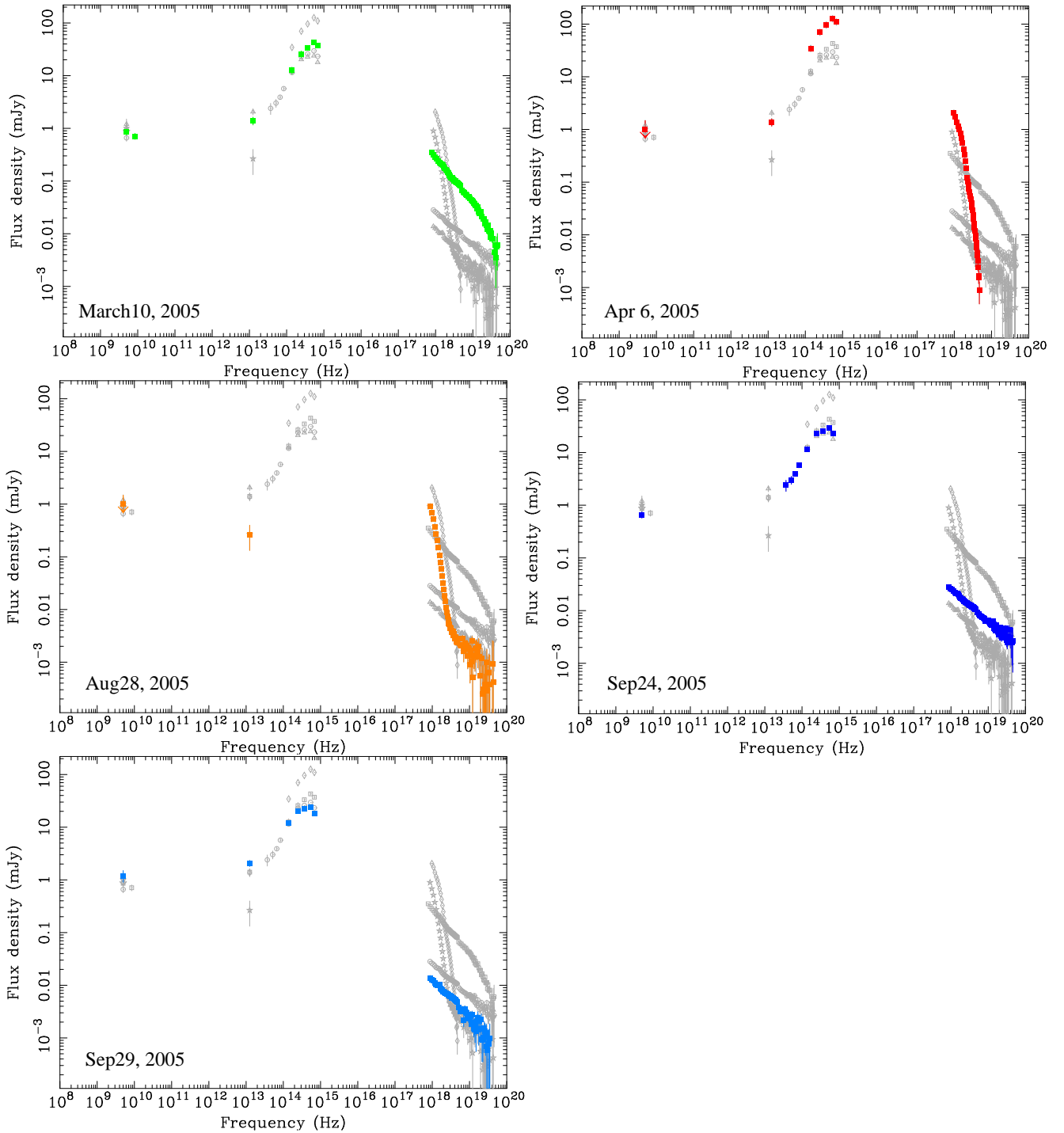


Fig. 4.— Broadband energy spectra of GRO J1655-40. The gray open markers show all the five spectra with Spitzer coverage during the outburst, and the filled markers highlight the observation on the date indicated in the bottom-left corner of each panel.

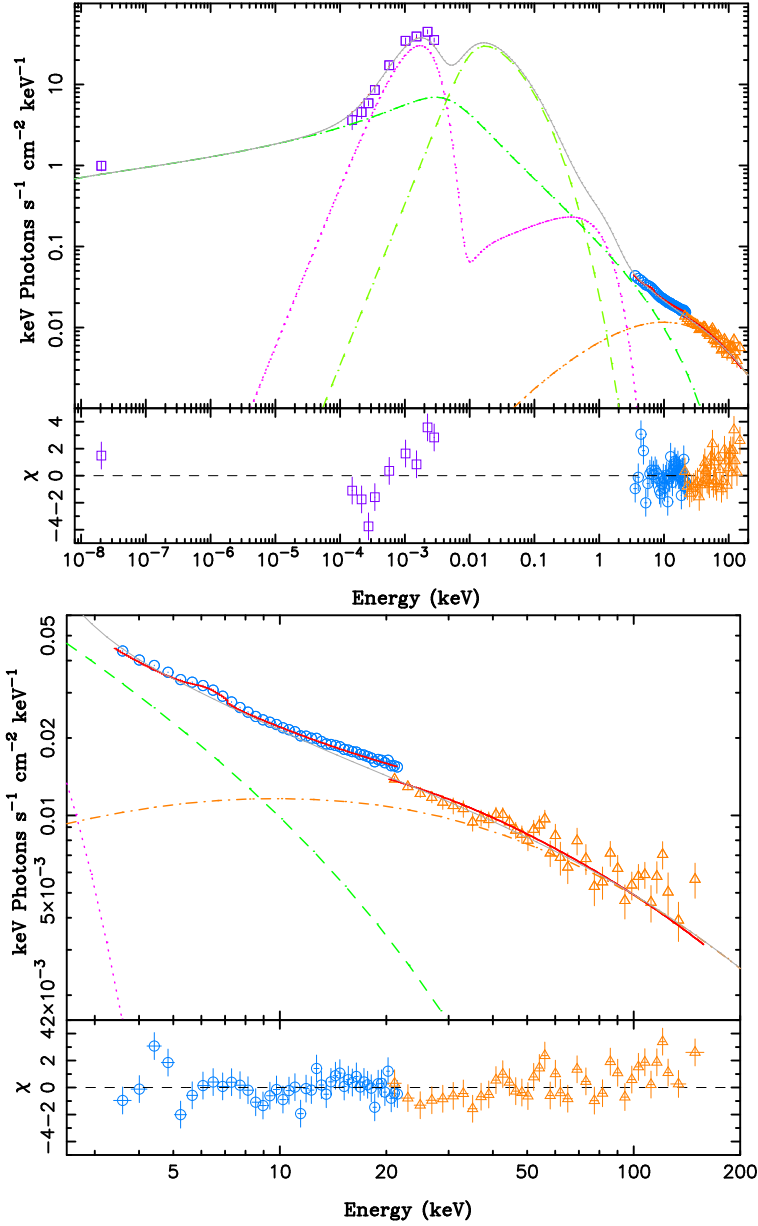


Fig. 5.— Jet model fits with residuals of the radio-to-X-ray (upper panel) and X-ray spectrum (lower panel) of the September 24 observation of GRO J1655-40, with the jet inclination angle fixed to 75° . The light green dashed line is the pre-shock synchrotron component, the darker green dash-dotted line is the post-shock synchrotron component, the orange dash-dotted line represents the SSC plus the disk external Compton component, the purple dotted line is the multi-temperature disk black body plus a black body representing the companion star in the binary system. The solid red line is the total model. Note that the model components in this representation are not absorbed and are not convolved with the response matrices.

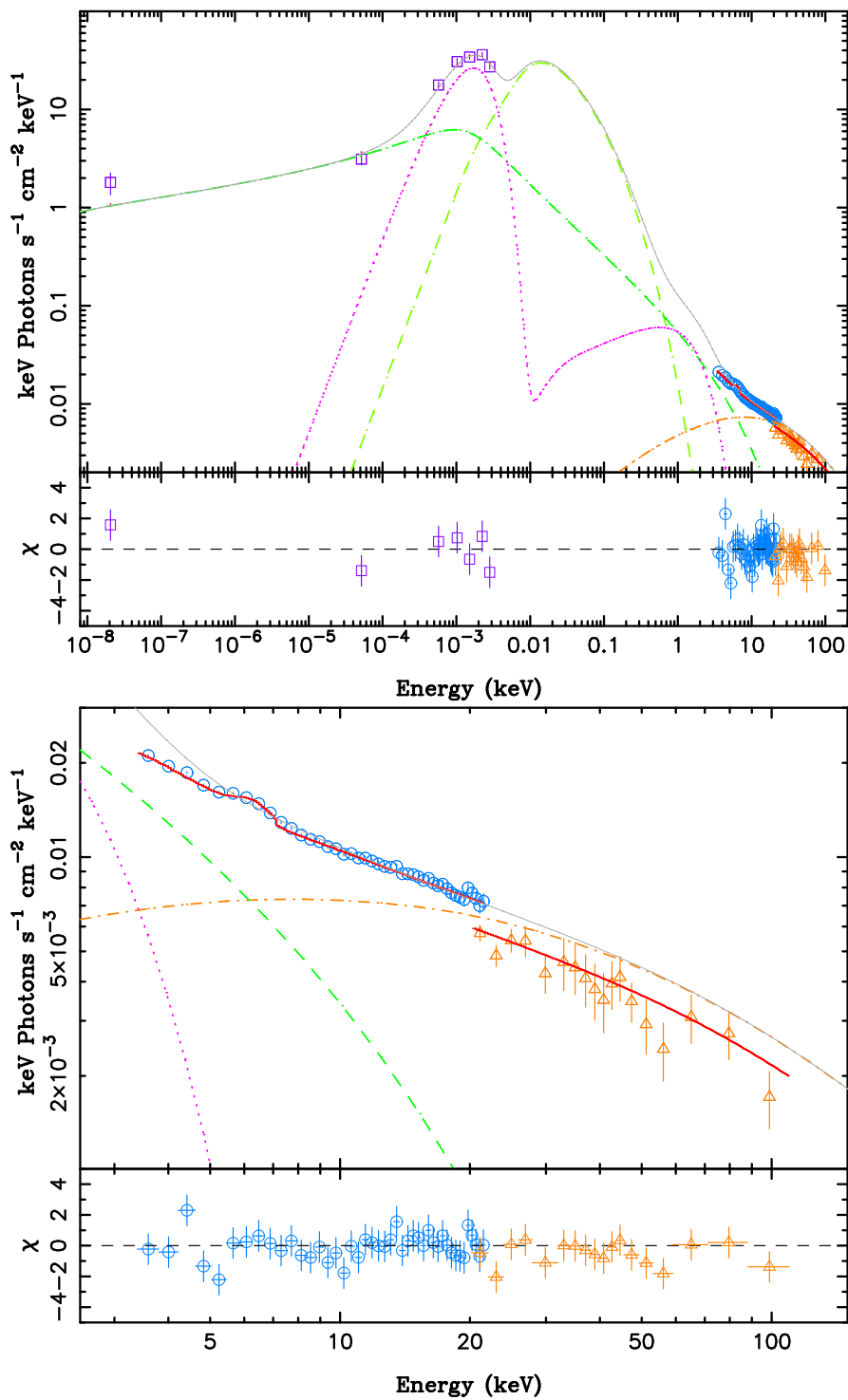


Fig. 6.— Jet model fits with residuals of the radio-to-X-ray (upper panel) and X-ray (lower panel) spectrum of the September 29 observation of GRO J1655-40, with the jet inclination angle fixed to 75°. Model components as in Fig. 5.

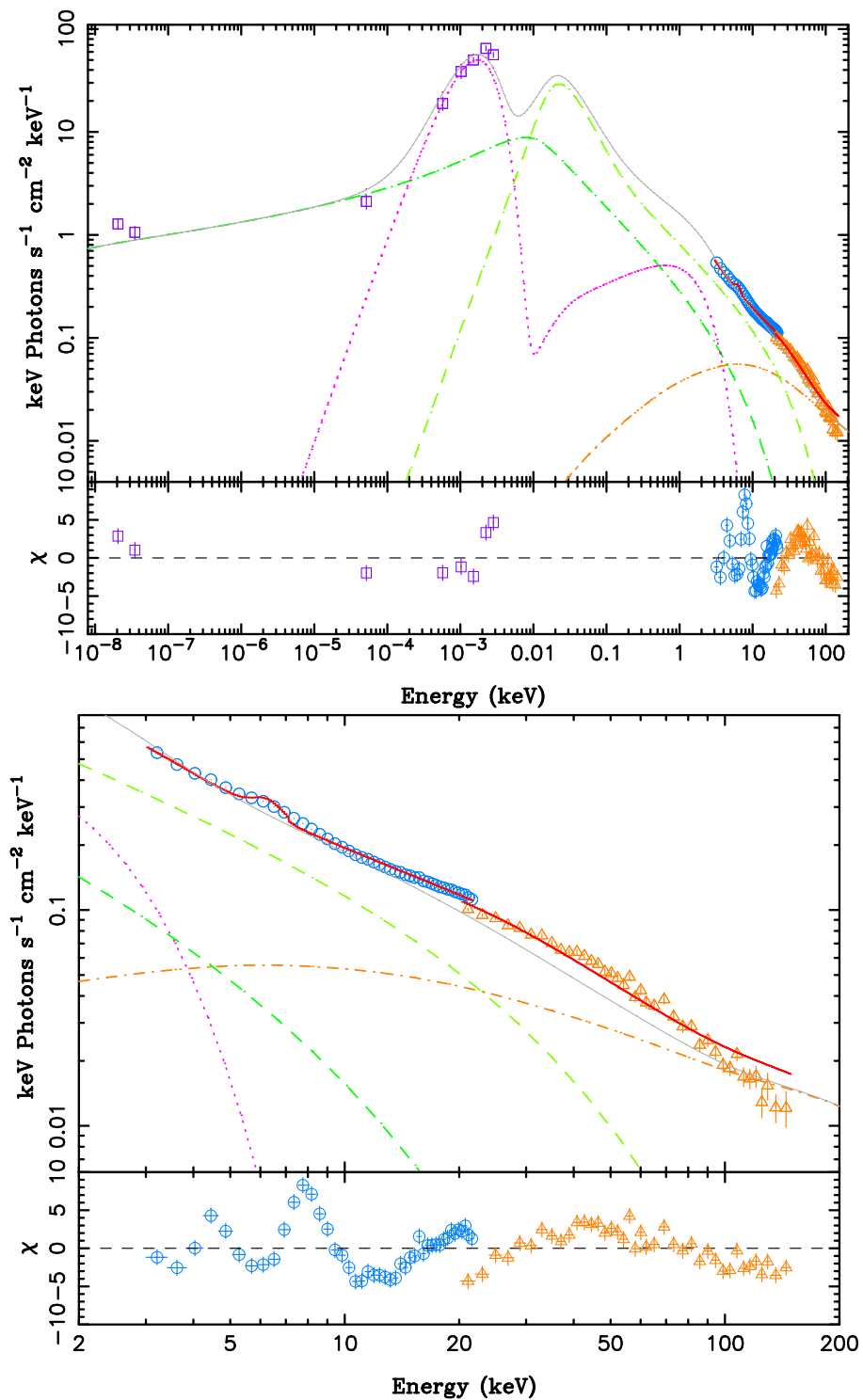


Fig. 7.— Jet model fits with residuals of the radio-to-X-ray (upper panel) and X-ray (lower panel) spectrum of the March 10 observation of GRO J1655-40, with the jet inclination angle fixed to 75° . Model components as in Fig. 5.

Table 1: Logs of the pointed RXTE and Spitzer simultaneous observations. Spitzer MIPS observations are at $24\ \mu\text{m}$, Spitzer IRAC are at 3.6 , 4.5 , 5.8 and $8\ \mu\text{m}$. For the Spitzer observations, we show the exposure time per pixel per Basic Calibrated Data (BCD), times the number of BCD frames used to create the mosaics.

RXTE			
Instrument	Start Obs.	End Obs.	ObsID
PCA/HEXTE	2005-03-10UT17:45:36	2005-03-10UT18:46:40	90704-04-01-00
PCA/HEXTE	2005-04-06UT00:47:28	2005-04-06UT01:53:36	91702-01-24-00
PCA/HEXTE	2005-04-06UT02:16:16	2005-04-06UT02:57:36	91702-01-24-02
PCA/HEXTE	2005-04-06UT10:27:12	2005-04-06UT10:50:40	91702-01-24-03
PCA/HEXTE	2005-08-28UT22:59:12	2005-08-29UT00:33:36	91702-01-47-10
PCA/HEXTE	2005-08-28UT12:08:48	2005-08-28UT13:12:48	91702-01-47-12
PCA/HEXTE	2005-08-28UT21:16:16	2005-08-28UT22:05:36	91702-01-46-12
PCA/HEXTE	2005-09-24UT05:42:24	2005-09-24UT11:23:44	91704-01-01-01
PCA/HEXTE	2005-09-29UT06:47:12	2005-09-29UT10:53:36	91702-01-87-02
Spitzer			
Instrument	Start Obs.	Exp. Time \times BCDs	ObsID
MIPS	2005-03-10UT18:13:34	9.96 s \times 70	10525184
MIPS	2005-04-06UT14:17:07	9.96 s \times 70	10525440
MIPS	2005-08-28UT11:43:36	9.96 s \times 70	10525696
IRAC	2005-09-23UT10:47:11	1.2 s \times 59	14508800
MIPS	2005-09-29UT02:43:03	9.96 s \times 70	14509312
MIPS	2006-04-01UT21:55:03	9.96 s \times 70	10524928

Table 2: Date, wavelength of observation, X-ray state and flux densities of the Spitzer MIPS observations at 24 μm and Spitzer IRAC at 3.6, 4.5, 5.8 and 8 μm . Errors are 1σ rms.

Date	Wavelength	X-ray state	Flux density (mJy)
2005 March 10	24 μm	hard/HIMS	1.40 ± 0.23
2005 April 6	24 μm	thermal	1.37 ± 0.22
2005 August 28	24 μm	thermal	0.26 ± 0.13
2005 September 23	3.6 μm	hard	5.67 ± 0.39
	4.5 μm		3.90 ± 0.29
	5.8 μm		3.02 ± 0.52
	8 μm		2.40 ± 0.57
2005 September 29	24 μm	hard	2.07 ± 0.27
2006 April 1	24 μm	quiescence	< 0.54

Table 3: Start time and apparent (non de-reddened) magnitudes of the B, V, I, J and K band observations of GRO J1655-40 with SMARTS. For each observing run, the exposure time is 6 minutes for the B, J and K bands, 4 minutes for the V band and 2 minutes for the I band. See also § 2.2.

Start Time	B mag	V mag	I mag	J mag	K mag
2005-03-09UT07:25:28	17.80	16.17	14.03	13.05	12.21
2005-03-10UT08:09:14	17.62	16.04	13.99	13.06	12.23
2005-04-05UT06:52:23	16.28	14.77	12.73	11.91	11.07
2005-04-06UT06:18:04	16.45	14.87	12.84	11.97	11.14
2005-04-07UT06:14:46	16.30	14.76	12.71	11.87	11.04
2005-09-22UT00:26:25	18.12	16.45	14.26	13.18	12.33
2005-09-28UT00:30:41	18.54	16.63	14.38	13.47	12.47
2005-09-29UT00:39:09	18.41	16.68	14.41	13.31	12.30
2005-09-30UT23:56:40	18.16	16.48	14.25	13.17	12.27

Table 4: Best-fit parameters of the RXTE energy spectra of GRO J1655-40. Errors are 68% confidence for one interesting parameter.

Parameter	Mar10	Apr6	Aug28	Sep24	Sep29
Disk Blackbody					
kT_{BB} (keV)	0.5 <i>fixed</i>	$1.25^{+0.01}_{-0.01}$	$0.87^{+0.01}_{-0.01}$	0.5 <i>fixed</i>	0.5 <i>fixed</i>
N_{BB}	1969^{+139}_{-140}	718^{+26}_{-29}	1904^{+15}_{-40}	115^{+29}_{-29}	106^{+18}_{-17}
Gaussian					
E_{Fe} (keV)	---	$6.24^{+0.07}_{-0.10}$	---	---	---
σ_{Fe} (keV)	---	0.1 <i>fixed</i>	---	---	---
N_{Fe} ($\times 10^{-3}$ phot. cm^{-2} s^{-1})	---	$9.02^{+0.01}_{-0.01}$	---	---	---
Power Law					
Γ_{PL}	$1.72^{+0.01}_{-0.01}$	$2.93^{+0.08}_{-0.07}$	$2.28^{+0.07}_{-0.05}$	$1.57^{+0.01}_{-0.01}$	$1.57^{+0.01}_{-0.02}$
N_{PL} (10^{-12} erg cm^{-2} s^{-1})	4296^{+13}_{-13}	5025^{+700}_{-636}	498^{+42}_{-39}	462^{+2}_{-2}	205^{+1}_{-1}
High-Energy Cutoff					
E_{cut} (keV)	33^{+3}_{-3}	$11.9^{+0.2}_{-0.2}$	---	---	---
E_{fold} (keV)	160^{+12}_{-11}	$4.6^{+0.3}_{-0.9}$	---	---	---
Smedge					
E_{edge} (keV)	$7.44^{+0.06}_{-0.06}$	$7.86^{+0.09}_{-0.06}$	$8.64^{+0.08}_{-0.07}$	$6.8^{+0.1}_{-0.1}$	$6.7^{+0.2}_{-0.2}$
Max τ	$1.81^{+0.05}_{-0.05}$	$1.0^{+0.3}_{-0.3}$	$5.0^{+0.4}_{-0.4}$	$1.46^{+0.08}_{-0.08}$	$0.6^{+1.2}_{-0.3}$
Width $_{edge}$ (keV)	> 10.6	$1.4^{+0.6}_{-0.5}$	> 8.7	> 7.5	$5.6^{+11.7}_{-2.8}$
Fit Statistics					
χ^2_{ν} (d.o.f.)	1.09 (85)	1.53 (38)	1.26 (85)	0.64 (86)	0.73 (86)

Table 5: Jet model best-fit parameters of the broadband energy spectra of GRO J1655-40 on 2005 September 24 and September 29, with a fixed distance of 1.7 kpc. One fit of the September 29 observation with a distance of 3.2 kpc is also shown. The best-fit parameters of two observations of GX 339-4 and Cyg X-1 from Markoff, Nowak & Wilms (2005) are reported for comparison. Errors are 90% confidence level. N_j is the jet normalization in Eddington luminosity units and is of the same order of the jet power, r_0 is the nozzle radius in gravitational radii units, T_e is the temperature of the pre-shocked electrons, p is the spectral index of the post-shock electron power-law distribution, k is the equipartition factor in units of the ratio between magnetic and electron energy density, pl_f is the fraction of accelerated electrons, z_{acc} is the location of the acceleration region in gravitational radii units, and h_0 is the radius-to-height ratio of the nozzle region. The u_{acc}/c parameter is the shock speed relative to the bulk plasma flow, f_{sc} is the ratio of the scattering mean free path to the gyroradius, L_{disk} is the disk luminosity in units of Eddington luminosity, T_{disk} is the inner disk temperature, A_{line} , E_{line} and σ_{line} are, respectively, the normalization, the peak energy and the width of the Gaussian emission line, and $\Omega/2\pi$ is the reflection fraction.

Date (jet incl./dist.)	N_j ($10^{-3} L_{Edd}$)	r_0 (GM/c^2)	T_e ($10^{10} K$)	p	k	pl_f	z_{acc}	h_0	
GRO J1655-40									
Sep24 (75°/1.7)	$2.91^{+0.01}_{-0.04}$	$3.48^{+0.01}_{-0.01}$	$4.82^{+0.02}_{-0.01}$	$2.50^{+0.01}_{-0.01}$	$4.17^{+0.01}_{-0.01}$	0.75 (fixed)	7 (fixed)	1.4 (fixed)	
Sep29 (75°/1.7)	$2.94^{+0.01}_{-0.02}$	$4.44^{+0.03}_{-0.02}$	$4.87^{+0.02}_{-0.03}$	$2.37^{+0.01}_{-0.01}$	$5.41^{+0.04}_{-0.02}$	0.75 (fixed)	20 (fixed)	1.2 (fixed)	
Sep29 (free/1.7)	$2.23^{+0.01}_{-0.01}$	$2.55^{+0.24}_{-0.11}$	$4.23^{+0.01}_{-0.04}$	$2.40^{+0.01}_{-0.01}$	$1.15^{+0.01}_{-0.05}$	0.75 (fixed)	20 (fixed)	1.2 (fixed)	
Sep29 (free/3.2)	$3.68^{+0.01}_{-0.01}$	$2.08^{+0.46}_{-0.08}$	$3.10^{+0.01}_{-0.01}$	$2.55^{+0.01}_{-0.01}$	$1.29^{+0.01}_{-0.02}$	0.75 (fixed)	10 (fixed)	1.5 (fixed)	
GX 339-4									
Apr2, 1999	$0.64^{+0.02}_{-0.03}$	$9.6^{+0.5}_{-0.1}$	$5.23^{+0.13}_{-0.12}$	$2.39^{+0.01}_{-0.01}$	$1.12^{+0.01}_{-0.01}$	$0.74^{+0.05}_{-0.01}$	302	$1.41^{+0.01}_{-0.01}$	
Cyg X-1									
Feb23, 2003	$0.74^{+0.01}_{-0.01}$	$4.4^{+0.2}_{-0.1}$	$3.28^{+0.01}_{-0.01}$	$2.61^{+0.01}_{-0.01}$	$1.77^{+0.04}_{-0.01}$	$0.73^{+0.08}_{-0.02}$	9	$1.18^{+0.01}_{-0.01}$	
Date (jet incl./dist)	u_{acc}/c	f_{sc}	L_{disk} ($10^{-3} L_{Edd}$)	T_{disk} (keV)	A_{line} (10^{-2})	E_{line} (keV)	σ_{line} (keV)	$\Omega/2\pi$	$\chi^2_{\nu} (dof)$
GRO J1655-40									
Sep24 (75°/1.7)	0.6 (fixed)	945^{+8}_{-51}	$0.36^{+0.39}_{-0.13}$	$0.39^{+0.12}_{-0.25}$	$0.04^{+0.01}_{-0.01}$	6.2 (fixed)	0.6 (fixed)	$0.36^{+0.13}_{-0.02}$	1.72 (81)
Sep29 (75°/1.7)	0.6 (fixed)	2450^{+58}_{-77}	$0.15^{+0.01}_{-0.01}$	$0.62^{+0.04}_{-0.02}$	$0.02^{+0.01}_{-0.01}$	6.2 (fixed)	0.5 (fixed)	< 0.01	0.90 (56)
Sep29 (free/1.7)	0.6 (fixed)	420^{+1}_{-8}	$0.07^{+0.01}_{-0.01}$	$0.59^{+0.01}_{-0.02}$	$0.02^{+0.01}_{-0.01}$	6.2 (fixed)	0.65 (fixed)	$0.37^{+0.03}_{-0.02}$	0.94 (55)
Sep29 (free/3.2)	0.6 (fixed)	631^{+336}_{-13}	$0.45^{+0.03}_{-0.03}$	$0.54^{+0.01}_{-0.02}$	$0.01^{+0.01}_{-0.01}$	$6.1^{+0.2}_{-0.1}$	0.65 (fixed)	$0.61^{+0.03}_{-0.07}$	1.20 (53)
GX 339-4									
Apr2, 1999	$0.32^{+0.05}_{-0.01}$	1100^{+200}_{-800}	$0.33^{+0.01}_{-0.01}$	$1.53^{+0.12}_{-0.10}$	$0.09^{+0.03}_{-0.03}$	$6.4^{+0.1}_{-0.1}$	$0.7^{+0.1}_{-0.1}$	< 0.06	1.76 (87)
Cyg X-1									
Feb23, 2003	$0.35^{+0.01}_{-0.01}$	790^{+10}_{-10}	$0.8^{+0.1}_{-0.1}$	$0.98^{+0.11}_{-0.09}$	$2.3^{+0.2}_{-0.5}$	$6.0^{+0.1}_{-0.1}$	$0.9^{+0.1}_{-0.1}$	< 0.01	1.17 (177)